

Mechanics Based Design of Structures and Machines

An International Journal

ISSN: 1539-7734 (Print) 1539-7742 (Online) Journal homepage: www.tandfonline.com/journals/lmbd20

Upgraded rocker pendulum-tuned mass damper for passive vibration control of structures

Huong Quoc Cao

To cite this article: Huong Quoc Cao (11 Jul 2025): Upgraded rocker pendulum-tuned mass damper for passive vibration control of structures, *Mechanics Based Design of Structures and Machines*, DOI: [10.1080/15397734.2025.2531076](https://doi.org/10.1080/15397734.2025.2531076)

To link to this article: <https://doi.org/10.1080/15397734.2025.2531076>



© 2025 The Author(s). Published with license by Taylor & Francis Group, LLC



Published online: 11 Jul 2025.



Submit your article to this journal [↗](#)



Article views: 158




View related articles [↗](#)



View Crossmark data [↗](#)

Upgraded rocker pendulum-tuned mass damper for passive vibration control of structures

Huong Quoc Cao 

School of Mechanical and Mechatronic Engineering, Faculty of Engineering and Information Technology,
University of Technology Sydney, New South Wales, Australia

ABSTRACT

An upgraded type of tuned mass damper for passive vibration control of structures is developed in this work. This innovative model includes a smaller tuned liquid column damper (TLCD) integrated into a rocker pendulum-tuned mass damper (RPTMD) placed on a smooth-curved surface of the main structure, which is referred to as the upgraded rocker pendulum-tuned mass damper (URPTMD). The URPTMD is a connectionless vibration absorber (CVA) because this design allows it to operate without connection to the main structure. This unique feature is an outstanding advantage of the URPTMD. This leads to easier installation and reduced maintenance costs. After establishing the analytical model of the URPTMD, the results obtained from the parametric studies indicate that the mass ratio between the TLCD and the RPTMD significantly affects the device's control performance. To explore the vibration reduction ability of this device, the performance of an optimized URPTMD are determined and compared with those of optimal TMD with the same weight. The numerical simulations show that the URPTMD yields higher effectiveness over a broader excitation frequency range compared with a conventional TMD. In addition, the robustness against changes in the structural properties and the mistuning sensitivity of the optimized URPTMD are also investigated. The URPTMD is less robust than the PTMD or TMD when facing changes in both structural stiffness and mass, but the damping sensitivity of the optimized URPTMD is similar to that of the optimized TMD.

ARTICLE HISTORY

Received 18 April 2025

Accepted 30 June 2025

KEYWORDS

Passive vibration control; upgraded rocker pendulum tuned mass damper; rocker pendulum tuned mass damper; connectionless vibration absorber; mistuning sensitivity; multi-objective optimization

1. Introduction

As construction technology advances, many high-rise buildings are increasingly being constructed around the world to optimize space usage. However, these structures are susceptible to significant amplitude vibrations caused by strong winds and earthquakes, primarily due to their high flexibility and low damping characteristics (Suthar and Jangid 2022; Li, Pan, and Cao 2022; Giaralis and Petrini 2017). In practice, one common technique is to add vibration absorbers to structures to mitigate structural dynamic responses (Samali et al. 2004; Wu et al. 2005; Gao, Kwok, and Samali 1999; Tran, Bui, et al. 2025). Following this way, tuned mass dampers (TMDs), including tuned liquid column dampers (TLCDs), are one of the most popular passive vibration absorbers (Gao,

CONTACT Huong Quoc Cao  huong.q.cao@student.uts.edu.au  School of Mechanical and Mechatronic Engineering, Faculty of Engineering and Information Technology, University of Technology Sydney, New South Wales, Australia
Communicated by Francesco Tornabene

© 2025 The Author(s). Published with license by Taylor & Francis Group, LLC

This is an Open Access article distributed under the terms of the Creative Commons Attribution-NonCommercial-NoDerivatives License (<http://creativecommons.org/licenses/by-nc-nd/4.0/>), which permits non-commercial re-use, distribution, and reproduction in any medium, provided the original work is properly cited, and is not altered, transformed, or built upon in any way. The terms on which this article has been published allow the posting of the Accepted Manuscript in a repository by the author(s) or with their consent.

Kwok, and Samali 1999; Diana et al. 2013; Momtaz, Abdollahian, and Farshidianfar 2017; Vellar, Gupta, and Jangid 2019; Yalla and Kareem 2000).

TMDs have widely been used to reduce vibrations of civil structures under different types of loads (e.g. earthquakes, wind or traffic loads). Researchers have developed various advanced types to enhance the vibration control capacity of traditional TMDs (Kahya and Araz 2019; Wang, Shi, and Zhou 2022; Hui et al. 2024; Zuo 2009). For instance, Cao developed a combined tuned mass damper (CTMD) (Cao 2023), while Tran and Bui introduced a rolling tuned mass damper (RTMD) designed to control vibrations in buildings subjected to earthquakes (Tran and Bui 2025). Additionally, Araz proposed connecting multiple TMDs in parallel, known as multiple tuned mass dampers (MTMD), to further reduce the dynamic responses of structures (Araz 2024). Recently, TMDs that utilize inerters have gained significant interest among scholars (Marian and Giaralis 2014; Pandey and Mishra 2021; Cao, 2025b; Prakash and Jangid 2022; Baduidana and Kenfack-Jiotsa 2024; Suthar and Banerji 2023; Tran, Bui, et al. 2025).

While traditional TMDs (or their innovative types) offer several advantages, including simple structure, low cost, and effective performance in reducing structural vibrations, they also present some drawbacks. One of these disadvantages is the large stroke of TMDs when they operate. Thus, TMDs may require huge horizontal installation spaces, which limits their practical applications for tall structures with space restrictions, particularly in slender high-rise buildings. To overcome this issue, pendulum tuned mass dampers (PTMDs), a special type of TMD, can be suitable for vibration reduction of slender civil structures due to the adequate installation space primarily in the vertical direction. Currently, PTMDs are being used to control the vibrations in tall buildings, and one of the typical examples of a PTMD installation is found in the Taipei World Financial Center (Taipei 101) in Taiwan.

The natural frequency of a PTMD is determined based on the length of the pendulum, and its design can be integrated with external dampers. To effectively control the vibrations of structures with very low natural frequencies, a significantly long pendulum is required to ensure that the pendulum's frequency matches with the natural frequency of the main structure. This requirement can result in complexity to the design of PTMD compared to a conventional Tuned Mass Damper (TMD), potentially lifting manufacturing costs. Furthermore, it is important to consider issues related to the bearings of a simple pendulum. To address these challenges, a more effective solution is to introduce a curvature in the support surface and allow the mass to roll on this surface (known as a rocker pendulum). This enables a rocker pendulum to operate similarly to a conventional pendulum.

Based on the above analyses, an upgraded type of TMD for passive vibration control is proposed in this work. This innovative version is a combination of a rocker pendulum-tuned mass damper (RPTMD) and a TLCD, which we refer to as the Upgraded Rocker Pendulum-Tuned Mass Damper (URPTMD). The URPTMD consists of a smaller TLCD mounted on top of an RPTMD, and the URPTMD is placed on a smooth-curved surface of the main structure. This design allows it to operate similarly to an upgraded TLCD (as presented in the paper by Cao (2021)) without connection to the main structure. In other words, URPTMDs are Connectionless Vibration Absorbers (CVA). This unique feature ensures that the URPTMD is different from conventional TMDs and other types of TMDs. Moreover, it simplifies installation and reduces maintenance costs. Additionally, the motion of the liquid column in the TLCD fixed to the URPTMD enhances the damping effect of the proposed device.

Beyond developing the analytical model for this new device, the main contributions of this study include outlining the fundamental characteristics of the URPTMD and evaluating its vibration control effectiveness, the robustness against variations in the structural parameters, and the mistuning sensitivity to changes in key properties of the URPTMD. To do this, an analytical model of a single-degree-of-freedom (SDOF) structure equipped with a URPTMD under an external force excitation is established in Section 2. Next, the parametric studies of the URPTMD

are conducted in Section 3, and then its optimal parameters are found in Section 4. The control performance and robustness of the URPTMD are determined and discussed in Section 5. The mistuning sensitivity of the device is also presented in Section 6. To the end, the outstanding findings of the present work are stated in Section 7.

2. Analytical model of the URPTMD-structure system

The natural frequencies of civil structures are generally distinct from one another. Thus, when vibration control of a specific vibration mode, the structure can be simplified to a SDOF system that shares the same frequency as the mode being controlled (Gao, Kwok, and Samali 1999). In the literature, many researchers have also focused on reducing the dynamic response of a specific vibration mode in high-rise buildings, simplifying their models by considering multiple-degree-of-freedom (MDOF) structures as SDOF structures (Gao, Kwok, and Samali 1999; Varadarajan and Nagarajaiah 2004; Yang et al. 2004). In this study, an analytical model is a SDOF structure equipped with a URPTMD under an external force $F(t)$ (as shown in Fig. 1a). The URPTMD

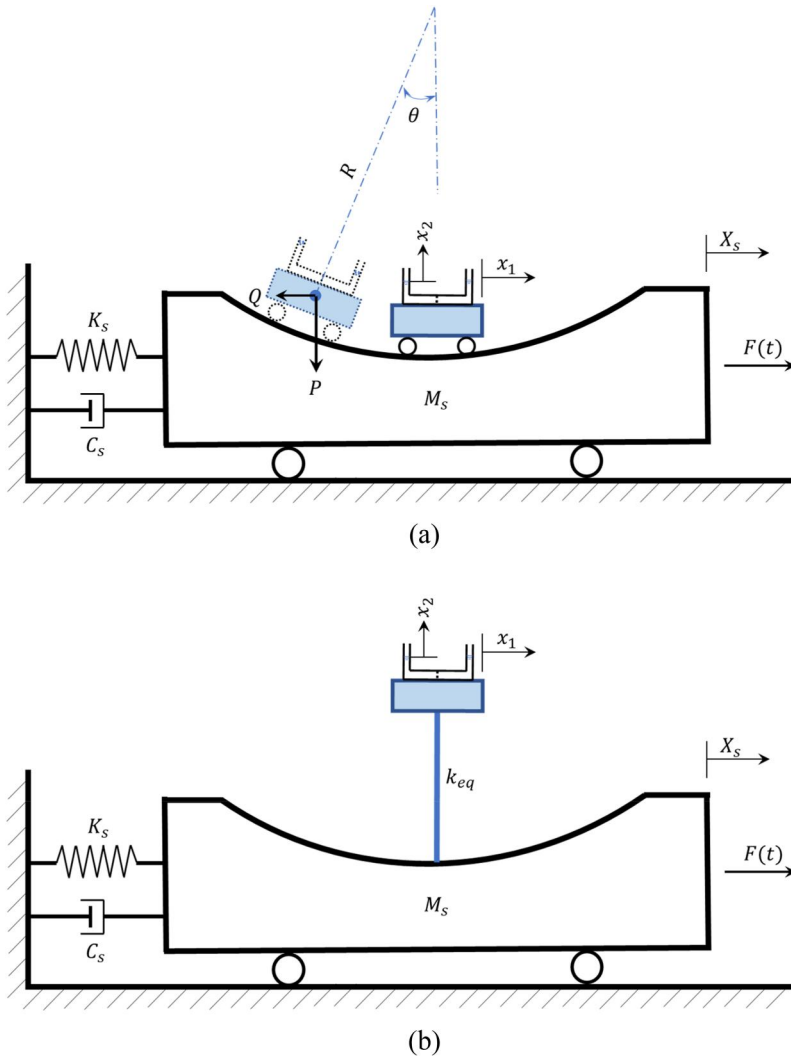


Figure 1. (a) Actual URPTMD-structure system, (b) Equivalent URPTMD-structure system.

consists of a TLCD integrated into a RPTMD. The mass of RPTMD is m_1 , while the TLCD is a uniform U-shaped liquid column which has a cross-sectional area (A), a head-loss coefficient (ζ), a total length (L), a horizontal length (B), and the liquid density (ρ). The key parameters of the main structure include the generalized stiffness (K_s), the mass (M_s) and the damping coefficient (C_s). The natural frequency and damping ratio of the structure are denoted as ω_s and ξ_s , respectively. They are calculated by $\omega_s = \sqrt{K_s/M_s}$ and $\xi_s = C_s/(2M_s\omega_s)$.

2.1. Equations of motion of the URPTMD-structure system

Figure 1a shows a URPTMD put on a smooth curved surface (e.g. a circular arc) of the main structure. The movement of the structure excites the pendulum. The motion of the pendulum produces a horizontal force that opposes the structure motion (Q). The horizontal force component due to the weight of the pendulum (P) will be a factor to pull the pendulum back to its initial equilibrium position. In the same mechanism, the URPTMD-structure system can be represented by an equivalent system, as presented in Fig. 1b.

In this study, the external force acting on the structure is assumed by

$$F(t) = F_0 e^{j\omega t}, \quad (1)$$

in which ω is the excitation frequency, F_0 is the force magnitude, and $j = \sqrt{-1}$. It is important to note that the equations of motion of the URPTMD for the case where the surface is a circular arc with the radius of R are the same as the conventional pendulum with the cable length of R . Here, θ (in radian) is denoted as the angle of oscillation of the URPTMD. It is assumed that θ is small ($\theta < 0.174$ rad) and the friction between URPTMD and the curved surface is neglected. Thus, equations of motion of the system are given by

$$M_s \ddot{X}_s(t) + C_s \dot{X}_s(t) + K_s X_s(t) - (\rho AL + m_1)g \sin(\theta(t)) = F(t), \quad (2a)$$

$$(\rho AL + m_1) \ddot{x}_1(t) + (\rho AL + m_1)g \sin(\theta(t)) = -(\rho AL + m_1) \ddot{X}_s(t) - \rho AB \ddot{x}_2(t), \quad (2b)$$

$$\rho AL \ddot{x}_2(t) + \frac{1}{2} \rho A \zeta |\dot{x}_2(t)| \dot{x}_2(t) + 2\rho A g x_2(t) = -\rho AB (\ddot{X}_s(t) + \ddot{x}_1(t)) \quad \text{with} \quad \left(|x_2(t)| \leq \frac{L-B}{2} \right). \quad (2c)$$

In the above equations, $g = 9.8 \text{ m/s}^2$ is the gravitational acceleration. $X_s(t)$ is the absolute displacement of the primary structure, $x_1(t)$ is the motion of the mass m_1 relative to M_s , and $x_2(t)$ is the vertical displacement of the liquid column. In other words, the absolute displacement of the mass m_1 is given by

$$x_1^{\text{abs}}(t) = x_1(t) + X_s(t). \quad (3)$$

As θ is small, the system is linearized and the following approximations can be applied

$$\sin(\theta) \approx \theta \quad \text{and} \quad \cos(\theta) \approx 1, \quad (4)$$

$$x_1 = R\theta \approx R\sin(\theta). \quad (5)$$

By substituting Equation (5) into Eqs. (2a-b), we obtain the equations of motion for the horizontal direction of the system as follows

$$M_s \ddot{X}_s(t) + C_s \dot{X}_s(t) + K_s X_s(t) - \frac{(\rho AL + m_1)g}{R} x_1(t) = F(t), \quad (6a)$$

$$(\rho AL + m_1)\ddot{x}_1(t) + \frac{(\rho AL + m_1)g}{R}x_1(t) = -(\rho AL + m_1)\ddot{X}_s(t) - \rho AB\ddot{x}_2(t), \quad (6b)$$

$$\rho AL\ddot{x}_2(t) + \frac{1}{2}\rho A\zeta|\dot{x}_2(t)|\dot{x}_2(t) + 2\rho Agx_2(t) = -\rho AB(\ddot{X}_s(t) + \ddot{x}_1(t)). \quad (6c)$$

It is noted that the mass of the liquid column in the TLCD (denoted as m_2) is calculated by $m_2 = \rho AL$. The length ratio of liquid column (denoted as γ) is given by $\gamma = \frac{B}{L}$. Here, the equivalent stiffness of the equivalent URPTMD-structure system is given by

$$k_{eq} = \frac{(m_1 + m_2)g}{R}. \quad (7)$$

Now, Eqs. (6a-6c) are rewritten as

$$M_s\ddot{X}_s(t) + C_s\dot{X}_s(t) + K_sX_s(t) - k_{eq}x_1(t) = F(t), \quad (8a)$$

$$(m_1 + m_2)(\ddot{X}_s(t) + \ddot{x}_1(t)) + k_{eq}x_1(t) = -\gamma m_2\ddot{x}_2(t), \quad (8b)$$

$$m_2\ddot{x}_2(t) + \frac{m_2\zeta}{2L}|\dot{x}_2(t)|\dot{x}_2(t) + m_2\frac{2g}{L}x_2(t) = -\gamma m_2(\ddot{X}_s(t) + \ddot{x}_1(t)), \quad (8c)$$

The natural frequency of the mass m_1 in the URPTMD is

$$\omega_1 = \sqrt{\frac{k_{eq}}{m_1}} = \sqrt{\frac{(m_1 + m_2)g}{m_1 R}} = \sqrt{\frac{(1 + m_2/m_1)g}{R}}, \quad (9)$$

The natural frequency of the TLCD in the URPTMD is

$$\omega_2 = \sqrt{\frac{2g}{L}}, \quad (10)$$

The mass ratio of the mass m_1 in the URPTMD is

$$\mu_1 = \frac{m_1}{M_s}, \quad (11a)$$

and the mass ratio of the liquid column in the URPTMD is

$$\mu_2 = \frac{m_2}{M_s}. \quad (11b)$$

Therefore, the mass ratio between the URPTMD and the structure is

$$\mu = \frac{m_1 + m_2}{M_s} = \mu_1 + \mu_2. \quad (11c)$$

Note that the mass ratio between the TMD2 and the TMD1 in the URPTMD is

$$\mu_{21} = \frac{\mu_2}{\mu_1} = \frac{m_2}{m_1}. \quad (11d)$$

It should be noted that Eq. (8c) is nonlinear because the damping term $\frac{\zeta}{2L}|\dot{x}_2(t)|$ in this equation is nonlinear. To directly solve Eqs. (8a-8c), Newmark's average acceleration method is applied. This method will be described in Appendix A.

2.2. Dynamic magnification factor of the structural response

The dynamic magnification factor (DMF) of the structural response in the steady state is expressed by (Den Hartog 1985; Gil-Martín et al. 2012)

$$DMF = \frac{\max X_s}{(F_0/K_s)} = \frac{\max X_s}{F_0/(M_s\omega_s^2)}. \quad (12)$$

In this work, letting the frequency ratio is

$$\alpha = \frac{\omega}{\omega_s}. \quad (13)$$

Two tuning frequency ratios of the proposed device are denoted as β_1 and β_2 . These tuning ratios are given by

$$\begin{cases} \beta_1 = \frac{\omega_1}{\omega_s} \\ \beta_2 = \frac{\omega_2}{\omega_s} \end{cases}. \quad (14)$$

It is evident that DMF of the structural response is a multi-variable function. With each structure given, two parameters ξ_s and α were determined, while the mass ratio μ will be pre-chosen by design engineers. The remaining parameters (including μ_{21} , β_1 , β_2 and ζ) will be found through optimization problems mentioned in the next section.

To assess the vibration control effectiveness of the proposed device, the TMD-structure system is also established for the purpose of comparisons. This system and its equations of motion are presented in [Appendix B](#).

3. Parametric study

In this section, studies on URPTMDs' parameters, which affect its vibration control performance, are carried out through numerical examples. In this study, the SDOF structure is the first mode of a 76-story building used in the literature (Varadarajan and Nagarajaiah 2004; Yang et al. 2004). The building has a total mass of 153000 tons. The first mode of the building has the natural frequency $\omega_s = 1.0$ (rad/s) and the damping ratio $\xi_s = 1\%$. It is assumed that the external force magnitude is $F_0 = 7.5 \times 10^5$ N and the excitation frequency range of $[\bar{\omega}_1, \bar{\omega}_2]$ corresponds to $0.5 \leq \alpha \leq 1.5$. Here, $\bar{\omega}_1$ and $\bar{\omega}_2$ are the lower and upper limits of the excitation frequency, respectively. This frequency range is chosen because it effectively captures the resonant and near-resonant behavior of the structure. In addition, the length ratio of the liquid column (γ) of UTLCD is fixed to be 0.75 for all cases considered.

3.1. Effects of the mass ratios μ and μ_{21}

The frequency response functions (FRF) of the structure (or the DMF_{max} curves of the structural response) for each value given of μ_{21} from 0.01 to 3.0 corresponding to the various values of μ are shown in [Fig. 2](#), in which the μ values are 0.01, 0.02, 0.03, 0.04 and 0.05. As shown in [Fig. 2](#), the remaining parameters include $\beta_1 = \beta_2 = 1$, $\gamma = 0.75$ and $\zeta = 50$. It is important to note that DMF_{max} is denoted as the peak dynamic magnification factor of the structural response in the excitation frequency range of $[\bar{\omega}_1, \bar{\omega}_2]$, and the lowest point of each DMF_{max} curve represents the maximum vibration reduction ability of URPTMD.

As observed in [Fig. 2](#), with any mass ratio, the vibration control performance of URPTMD is significant if the value of μ_{21} is small (it should be less than 1.0). In contrast, the URPTMD will not be effective if μ_{21} chosen is large. The second observation is that, based on the lowest point

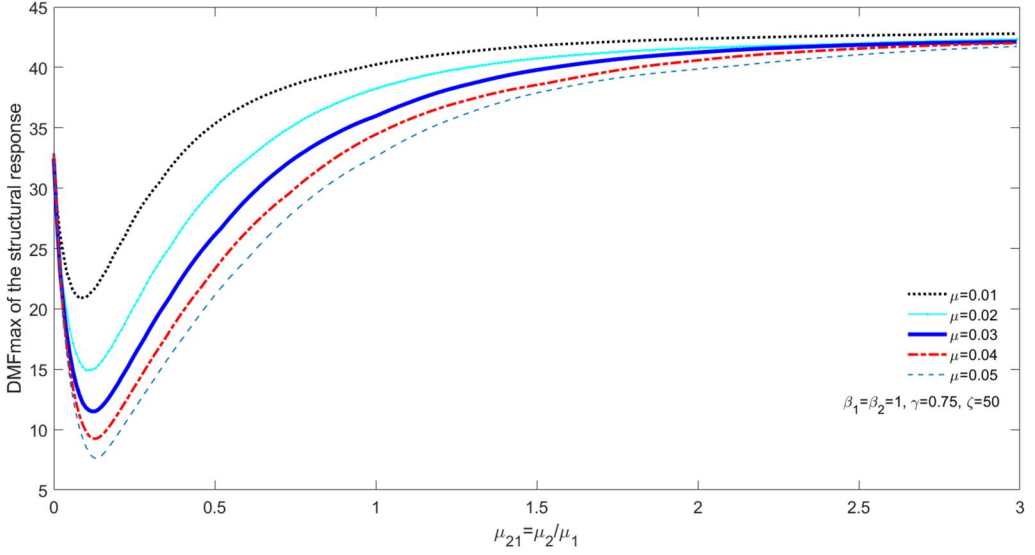


Figure 2. DMF_{max} curves of the structure response for various cases of μ_{21} .

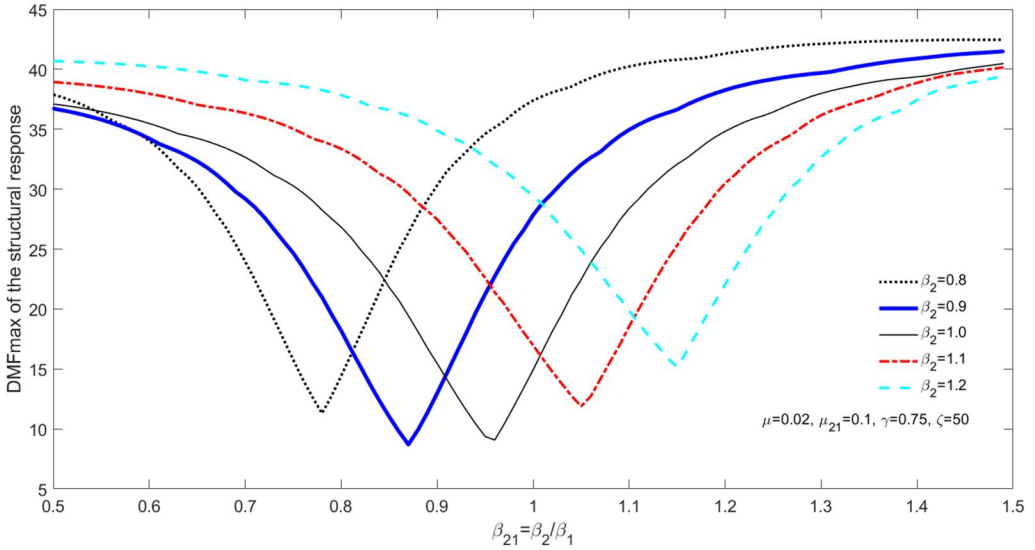


Figure 3. DMF_{max} curves corresponding to different values of β_2 .

of DMF_{max} curves in Fig. 2, the vibrational reduction capacity of the proposed device will rise when the mass ratio μ increases. In particular, the lowest point of DMF_{max} curve decreases from 20.93 to 7.615 when μ rises from 0.01 to 0.05. Furthermore, the optimal value of μ_{21} can be determined for each μ given, and this value of μ_{21} will be larger if one uses a larger mass ratio. For example, the optimum μ_{21} value obtained is 0.09 at $\mu = 0.01$, and the optimal value of μ_{21} continuously increases to 0.13 when μ continuous to rise to 0.05.

3.2. Effects of the tuning ratios β_1 and β_2

To survey the effects of the tuning ratios, let us consider the tuning ratio of URPTMD ($\beta_{21} = \beta_2/\beta_1$) changes in the domain of $[0.5, 1.5]$ while μ and μ_{21} are fixed at 0.02 and 0.1,

respectively. In addition, the head-loss coefficient of the TLCD in the URPTMD is assumed to be 50. The effect of the tuning ratio β_{21} on the DMF_{max} curve is shown in Fig. 3 with different values of β_2 . As observed in Fig. 3, there exists the lowest point in each DMF_{max} curve corresponding to each value of β_2 . Based on the observation of the lowest point of each DMF_{max} curve in Fig. 3, it can be seen that the β_{21} value rises as β_2 increases. Particularly, the lowest point of the DMF_{max} curve is from 8.697 to 15.16, while the β_{21} value rises from 0.78 to 1.15 when β_2 varies from 0.8 to 1.2. Thus, one can determine the optimal values of β_2 and β_1 based on minimizing the smallest value of the DMF_{max} curve.

3.3. Effects of the head-loss coefficient

Figure 4 describes the effects of the coefficient of head loss (ζ) on changes in the DMF_{max} curve in the case of the tuning ratio $\beta_2=1.0$, in which the values of ζ are 25, 50, 75, 100 and 125, respectively. It should be noted that this survey is for the case of $\mu = 0.02$ and $\mu_{21}=0.1$. One can observe from Fig. 4 that the control performance of the URPTMD will reduce when the head loss coefficient increases from 25 to 125. Namely, the smallest value of the DMF_{max} curve is 7.61 at $\zeta = 25$, and this value increases to 13.57 at $\zeta = 125$. However, with such a broad range of the ζ value (from 25 to 125), changes in the minimum DMF_{max} values of the DMF_{max} curves are small. This means that the sensitivity to change of ζ is small, and this point will be verified in Section 6.1 (the sensitivity of the head-loss coefficient).

In conclusion, every DMF_{max} curve in the above analyses has a nadir. Therefore, we can find a set of proper values of β_1, β_2, ζ , and μ_{21} to maximize the structural vibration control capacity of a URPTMD. To do this, a parametric optimization procedure will be introduced in the next section.

4. Parametric optimization

The core aim of the parametric optimization is to maximize the vibration absorption capacity of the damper. This means that the maximum value of the dynamic magnification factor (denoted as DMF_{max}) of the structural response when the excitation frequency changes in the domain $[\bar{\omega}_1, \bar{\omega}_2]$ should be minimized. Therefore, the objective function based on the value of DMF_{max} is given by

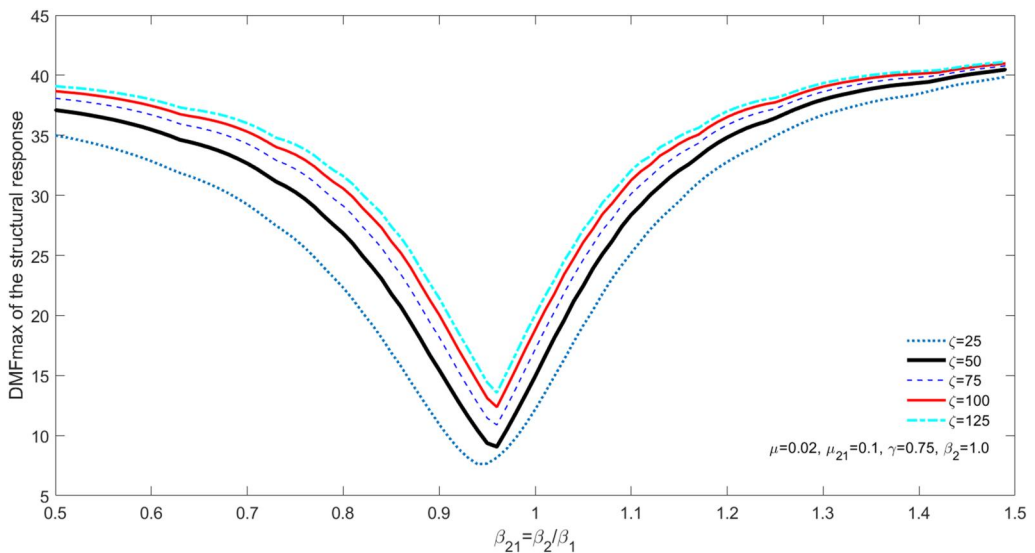


Figure 4. DMF_{max} curves for different ζ values.

$$\left(DMF_{max} \left| \begin{array}{c} \bar{\omega}_2 \\ \bar{\omega}_1 \end{array} \right. \right) \rightarrow \min \quad (15)$$

It should be noted that the value of DMF_{max} in the frequency range of $[\bar{\omega}_1, \bar{\omega}_2]$ is determined by (Gao, Kwok, and Samali 1999; Yamaguchi and Harnpornchai 1993)

$$DMF_{max} \Big|_{\bar{\omega}_1}^{\bar{\omega}_2} = \frac{\max \left(X_s \Big|_{\bar{\omega}_1}^{\bar{\omega}_2} \right)}{(F_0/K_s)} = \frac{\max \left(X_s \Big|_{\bar{\omega}_1}^{\bar{\omega}_2} \right)}{F_0/(M_s \omega_s^2)}. \quad (16)$$

Eq. (15) is a multi-variable objective function with many constraints. Thus, to solve this problem, we need a potential optimization algorithm.

In the literature, there are techniques developed to solve optimization problems (McCall 2005; Etedali and Rakhshani 2018; Le-Duc, Nguyen, and Nguyen-Xuan 2020). One can use one of the existing algorithms such as Genetic Algorithms, Cuckoo Search Algorithm, Firefly Algorithm and Moth-Flame Optimization to optimize the design of URPTMD. Among the recently introduced optimization algorithms, Balancing Composite Motion Optimization (BCMO) is a novel technique developed by Le-Duc et al. (Le-Duc, Nguyen, and Nguyen-Xuan 2020). Basically, the BCMO is a population-based optimization algorithm and its basic principles were explained in detail in Ref. (Le-Duc, Nguyen, and Nguyen-Xuan 2020). Moreover, scholars can find the MATLAB source codes of this algorithm in Ref. (Le-Duc, Nguyen, and Nguyen-Xuan 2020) through the link the authors provided. Thanks to high efficiency, low complexity, and rapid convergence compared to various population-based optimization algorithms (Le-Duc, Nguyen, and Nguyen-Xuan 2020; Bui, Tran, et al. 2023; Bui, Tran, et al. 2023; Cao, Tran, and Bui 1984; Tran, Bui, and Cao 2024), the BCMO is chosen to search the optimal parameters for devices in the present work.

The BCMO algorithm has two important parameters. They include the number of generations (N_G) and the number of individuals in the population (N_P). These parameters are selected based on the number of variables of the objective function and the convergence of that function. Additionally, a flowchart of the design optimization procedure for the URPTMD is depicted in

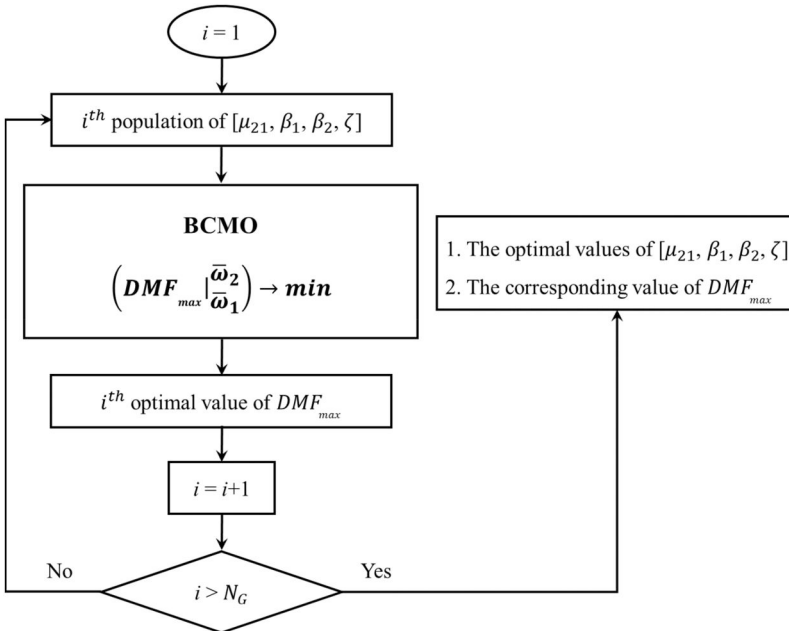


Figure 5. Design optimization procedure of the URPTMD with the BCMO algorithm.

Table 1. The lower and upper limits of the parameters of the URPTMD.

Parameter/Design variable	Value	Notation and expression
μ_{21}	$0.01 < \mu_{21} < 1.0$	$\mu_{21} = \frac{m_2}{m_1}$
β_1	$0.5 < \beta_1 < 1.5$	$\beta_1 = \frac{\omega_1}{\omega_s}$
β_2	$0.5 < \beta_2 < 1.5$	$\beta_2 = \frac{\omega_2}{\omega_s}$
ζ	$10 < \zeta < 300$	The head-loss coefficient of the TLCD

Table 2. Optimal parameters of URPTMD and TMD corresponding to each given value of μ .

URPTMD						TMD	
μ_{URPTMD}	μ_{21opt}^{URPTMD}	β_{1opt}^{URPTMD}	β_{2opt}^{URPTMD}	ζ_{opt}^{URPTMD}	R_{opt}^{URPTMD}	β_{tmd}^{opt}	ζ_{tmd}^{opt}
1.0%	0.050	1.023	0.985	9.715	9.84	0.989	0.062
1.5%	0.068	1.028	0.977	17.194	9.90	0.983	0.075
2.0%	0.093	1.039	0.970	30.421	9.92	0.978	0.086
2.5%	0.114	1.047	0.964	43.930	9.96	0.973	0.096
3.0%	0.138	1.057	0.957	62.092	9.98	0.968	0.105
3.5%	0.152	1.061	0.950	73.978	10.02	0.963	0.114
4.0%	0.180	1.073	0.945	99.350	10.04	0.959	0.121
4.5%	0.200	1.080	0.939	120.031	10.08	0.954	0.128
5.0%	0.228	1.091	0.935	148.483	10.11	0.949	0.135

Fig. 5. It is noted that the URPTMD has four design variables (including μ_{21} , β_1 , β_2 and ζ) that should be optimized. These design variables and their lower and upper bounds are listed in Table 1.

It is noted that the head-loss coefficient (ζ) of the TLCD which depends on the orifice opening ratio has a maximum limit. In previous works, Wang et al. used a head-loss coefficient value of 2000 (Wang et al. 2020), while Pandey and Mishra (Pandey and Mishra 2021) assumed a ratio of the head-loss coefficient to the length of the TLCDI (ζ/L) to be 161. However, manufacturing a TLCD with a very large value of ζ is challenging. Therefore, in this study, the maximum head-loss coefficient for URPTMD is limited at 300.

For extensive comparisons between the proposed device (URPTMD) and TMD, a model of the TMD-structure system is also established, as shown in Appendix B. It should be noticed that URPTMDs are connectionless vibration absorbers, and they are different from conventional TMDs and other types of TMDs. However, comparing the URPTMD with the TMD is appropriate because (1) both URPTMD and TMD have the same fundamental principle of a tuned vibration absorption, (2) TMD is highly effective for harmonic excitations and is considered a benchmark damper among tuned vibration absorbers, and (3) an optimal TMD offers equivalent effectiveness as an optimized PTMD (or RPTMD) if the natural frequency, mass and damping coefficient of the PTMD (or RPTMD) are designed to be the same as those of the TMD. In particular, a rocker pendulum operates similarly to a conventional pendulum, while the analogy between a TMD and a PTMD (as reported in Ref. (Soltani and Deraemaeker 2022)) enables the application of all tuning rules developed for TMDs in the case of PTMDs. Moreover, the results obtained in the research work (Wang et al. 2023) show that the control effectiveness of an optimal PTMD is similar to that of an optimized TMD with the same weight as the PTMD. This means that a comparison between the URPTMD and the TMD is also a comparison between the URPTMD and the PTMD (or RPTMD).

From the input data in Section 3 and Table 1 and using the BCMO algorithm with the corresponding parameters $N_p=300$ and $N_G=200$, Table 2 lists the obtained parameters of the optimal URPTMD and TMD configurations corresponding to each μ value given (including $\mu=1\%$, 1.5% , 2% , 2.5% , 3% , 3.5% , 4% , 4.5% and 5%). It should be noticed that the optimal radius of the

circular arc (curved surface) for URPTMD moving (R_{opt}^{URPTMD}) is also provided in Table 2. It is observed from Table 2 that the optimal values of μ_{21opt}^{URPTMD} , β_{1opt}^{URPTMD} , ζ_{opt}^{URPTMD} and R_{opt}^{URPTMD} increase while β_{2opt}^{URPTMD} reduces as the mass ratio is from 1% to 5%. For the optimal TMD configurations (as shown in Table 2), there is a decrease in the optimal values of β_{tmd}^{opt} , while the remaining parameter ζ_{tmd}^{opt} increases when the μ value rises. In this optimization problem, to ensure the global convergence of the optimal values, each URPTMD configuration is independently run five times, and the standard deviations of the results are consistently under 0.3%.

On the other hand, the optimal μ_{21opt}^{URPTMD} values obtained are small. These values are consistent with the conclusion in Section 3 that the performance of URPTMD is significant if $\mu_{21} < 1.0$ with any mass ratio. In addition, to validate the optimal parameters of the devices obtained using the BCMO algorithm, we can use the explicit formulas of Den Hartog (Den Hartog 1985) to compute optimal parameters of TMD applied to SDOF structures. In particular, the optimal damping ratio (ζ_t) is calculated by $\zeta_{tmd} = \sqrt{\frac{3\mu}{8(1+\mu)}}$, and the optimal frequency ratio (β_t) is determined by $\beta_{tmd} = \frac{1}{(1+\mu)}$. From the data presented in Table 2, the optimal parameters of the TMD with the BCMO algorithm match well with those of the TMD gained by using the explicit formulas of Den Hartog.

5. Effectiveness and robustness

To evaluate the vibration control capability and the robustness of an optimal URPTMD, the performance and robustness of the optimized URPTMD are calculated and compared with those of optimum TMD which has the same weight as the URPTMD.

5.1. Control performance of URPTMD

In this section, two criteria for evaluating the vibration suppression ability of URPTMD or TMD are the DMF_{max} value of the structural response (Gao, Kwok, and Samali 1999; Yamaguchi and Harnpornchai 1993) and the root mean square (RMS) of the peak displacement response (RMS_X) of the structure (Cao 2023; Cao, 2025a). For the first criterion, a vibration absorber with a smaller value of DMF_{max} is more effective (Gao, Kwok, and Samali 1999; Yamaguchi and Harnpornchai 1993). Meanwhile, the second one is related to the vibrating energy dissipated, and a smaller value of RMS_X means that more vibrating energy is dissipated by the device (Cao 2023; Cao, 2025a). In this study, the dimensionless quantity of RMS_X in the frequency range $[\bar{\omega}_1, \bar{\omega}_2]$ is expressed by (Cao 2023; Cao, 2025a):

$$RMS_X = \sqrt{\frac{\sum_1^n (\bar{X}_i)^2}{n}} = \sqrt{\frac{\sum_1^n \left(\frac{X_i}{F_0/K_s}\right)^2}{n}} = \sqrt{\frac{\sum_1^n \left(\frac{X_i}{F_0/(M_s \omega_s^2)}\right)^2}{n}}, \quad (17)$$

where X_i is the sampling value of the structural peak displacement at the excitation frequency ω_i in the above frequency range. It should be noticed that Equation (17) are also used for computing the RMS displacement of the liquid column of the TLCD and RPTMD in the URPTMD.

Denoting “UC” as the uncontrolled structure and “device” as the structure equipped with the device, based on the DMF_{max} value, the vibration reduction of the structure controlled by each device can be defined by

$$R_{DMF} = \frac{DMF_{max}^{UC} - DMF_{max}^{device}}{DMF_{max}^{UC}} \times 100\%. \quad (18)$$

And based on the RMS_X index, the vibrating energy reduction of the structure controlled by each device can be calculated by

$$R_{RMS} = \frac{RMS_{\bar{X}}^{UC} - RMS_{\bar{X}}^{device}}{RMS_{\bar{X}}^{UC}} \times 100\%. \quad (19)$$

It is noted that the uncontrolled structure has the values of DMF_{max} and $RMS_{\bar{X}}$ are 50.0 and 8.795, respectively. Based on the optimal configurations of URPTMD and TMD in Table 2, the values of DMF_{max} , R_{DMF} , $RMS_{\bar{X}}$ and R_{RMS} of these configurations are reported in Table 3. As discussed earlier, a device with a smaller DMF_{max} value is more effective. It is found from Table 3 that URPTMD's optimal configuration offers smaller values of DMF_{max} and R_{DMF} compared to those of TMD with the same μ given. Furthermore, as previously mentioned in Section 4, the control performance of an optimal PTMD is similar to that of an optimized TMD with the same weight as the PTMD (Wang et al. 2023). Thus, it can be concluded that a URPTMD is more effective than a PTMD or a conventional TMD with the same weight. In particular, the vibration control effectiveness improvement of the optimal URPTMD configurations compared to the TMD configurations are from 19.3% to 22.4% (based on the DMF_{max} index) and from 5.1% to 6.9% (based on the $RMS_{\bar{X}}$ index) when μ rises from 0.01 to 0.05.

To make the discussion clearer, Fig. 6 shows the control effectiveness of the URPTMD and TMD for the different mass ratios, in which Fig. 6a is for the DMF_{max} values and Fig. 6b is for the values of $RMS_{\bar{X}}$. It should be noted that the vibration control performance and weight of an absorber added to the structure are constantly subjected to the law of trade-off. In other words, an increase in the control effectiveness of the device comes with a larger weight added to the main structure. It is found from Table 3 and Fig. 6 that the effectiveness of the URPTMD at $\mu = 2.5\%$ is similar to that of the TMD at $\mu = 4.5\%$ based on the DMF_{max} value (6.08 and 6.05, respectively). This also means that using the optimal URPTMD with $\mu = 2.5\%$ rather than a TMD (or a PTMD) with $\mu = 4.5\%$ can reduce the damper's mass added to the structure by at least 2% of the total mass of the structure. In another case, the optimal TMD with $\mu = 3.5\%$ is not as effective as the optimized URPTMD at $\mu = 2\%$ based on the DMF_{max} index (6.75 compared to 6.72).

On the other hand, due to the safety of the main structure, the mass of the URPTMD added to the structure (which is usually determined through the mass ratio μ) is limited. Generally, the weight of the vibration absorber can be chosen from 1% to 5% of the mass of the main structure (Ocak et al. 2022; Rao 2017). The mass ratio range of 1% to 5% is suitable because it effectively balances the control performance, practical implementation conditions, typical structural characteristics and structural safety. However, increasing the mass ratio comes with trade-off, including higher structural loads, increased costs, greater system complexity, spatial constraints, and diminished control benefits. As observed in Fig. 6, the slope of the DMF_{max} curve decreases when the mass ratio increases from 1% to 5%. In other words, the control performance gain reduces when the value of μ rises. With a mass ratio greater than 5%, the additional reduction in the structural vibration amplitude becomes less significant. This is why the mass ratio range of [1%, 5%] is used to survey the control effectiveness of the proposed device in this work.

Table 3. DMF_{max} , $RMS_{\bar{X}}$ and R_{DMF} , R_{RMS} reduction (%) of each device for various cases of μ .

μ	URPTMD				TMD			
	DMF_{max}	R_{DMF}	$RMS_{\bar{X}}$	R_{RMS}	DMF_{max}	R_{DMF}	$RMS_{\bar{X}}$	R_{RMS}
1.0%	9.18	81.6%	4.59	47.8%	11.36	77.3%	4.84	45.0%
1.5%	7.61	84.8%	4.23	51.9%	9.65	80.7%	4.46	49.3%
2.0%	6.72	86.6%	3.95	55.1%	8.56	82.9%	4.21	52.2%
2.5%	6.08	87.8%	3.75	57.3%	7.80	84.4%	4.00	54.5%
3.0%	5.62	88.8%	3.60	59.1%	7.21	85.6%	3.84	56.3%
3.5%	5.25	89.5%	3.48	60.5%	6.75	86.5%	3.72	57.7%
4.0%	4.95	90.1%	3.36	61.8%	6.37	87.3%	3.60	59.0%
4.5%	4.70	90.6%	3.27	62.8%	6.05	87.9%	3.50	60.2%
5.0%	4.49	91.0%	3.18	63.8%	5.78	88.4%	3.42	61.1%

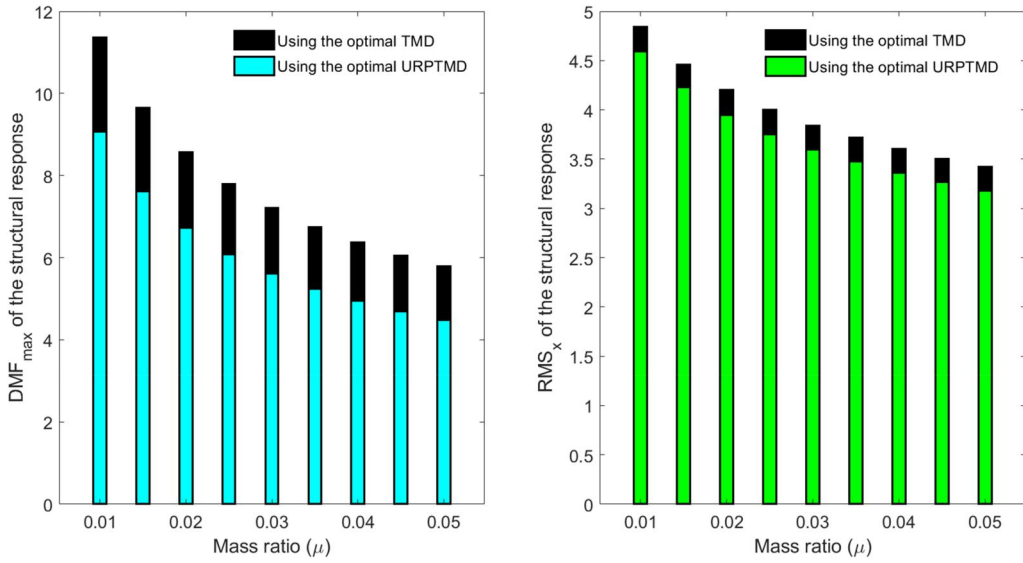


Figure 6. The control effectiveness of the URPTMD and TMD for the different mass ratios: (a) based on the DMF_{max} values, and (b) based on the RMS_x values.

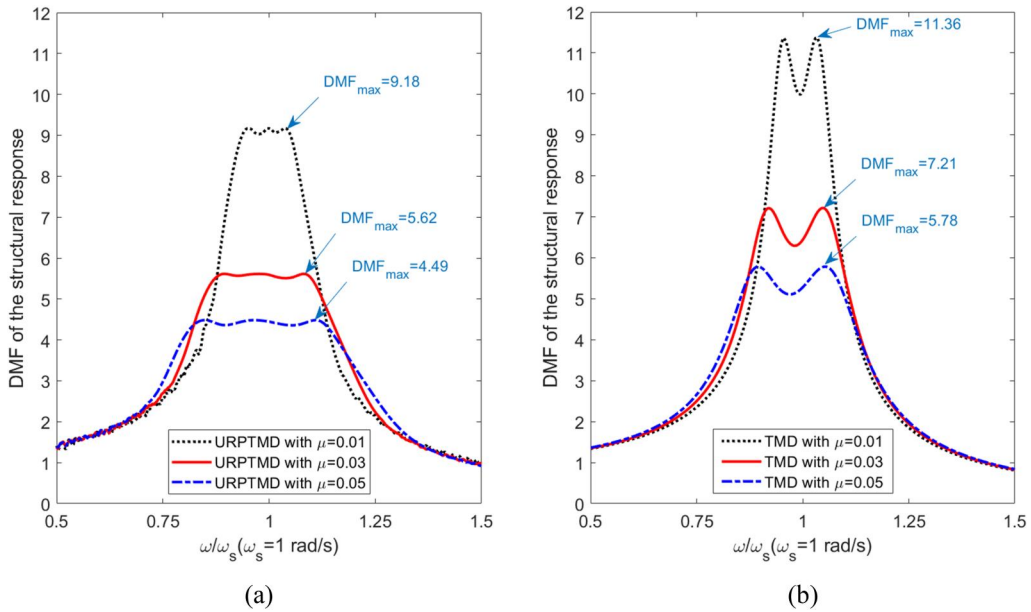


Figure 7. DMF curves of the structure controlled by (a) the URPTMD or (b) TMD with the different values of μ .

FRF curves of the structure equipped with the optimal URPTMD configurations are shown in Fig. 7a, while such curves of the structure with the TMDs are presented in Fig. 7b for the cases of $\mu = 1\%$, 3% and 5%. It is observed in Fig. 7 that, with the same mass ratio, the system with the URPTMD always yields a significantly smaller DMF_{max} value compared to the system using the TMD. The second observation from Fig. 7 is that the DMF curve of the structure with the URPTMD has three-peak characteristics, while the DMF curve of the structure with the TMD has two-peak characteristics. With the same value of μ , the three-peak DMF curve of the structure coupled with the URPTMD is relatively flat on a broader frequency range compared to the two-peak DMF curve of the structure equipped with

the TMD. Therefore, it can be concluded that, for passive vibration control of the structure, the optimal URPTMD configuration is much more effective than the optimized TMD or PTMD with the same weight.

When the primary structure vibrates due to the external force excitation, a part of the vibrational energy from the structure is transferred to the URPTMD. This energy part can be referred to as damping energy. The damping energy is then distributed among the components of the URPTMD (including the TLCD and RPTMD), and becomes the vibrational energy of the device. As discussed earlier, the RMS displacement is related to the vibration energy. To have a clearer look at distributing damping energy across the TLCD and RPTMD components of the URPTMD, the values of RMS displacement of the RPTMD and of the liquid column in the TLCD are determined using Equation (17). These values are listed in Table 4, in which RMS_{x1}^{RPTMD} and RMS_{x2}^{TLCD} are denoted as RMS displacement of the RPTMD and of the liquid column in the TLCD, respectively.

It can be seen from Table 4 that the RMS displacement of the TLCD in the URPTMD is always larger than that of the RPTMD for each given mass ratio. This means that the TLCD plays an important role in dissipating the vibration energy transferred from the main structure. The vibrational energy dissipated by the TLCD is mainly through the orifice, which is quantified by the nonlinear damping term. The energy dissipation is influenced by the liquid velocity and is maximized when the URPTMD is optimally tuned.

5.2. Robustness of URPTMD

The natural frequency of the main structure depends on the stiffness and mass (K_s and M_s), and any changes in K_s and/or M_s always lead to a change in the structural natural frequency. In practical applications, the structural stiffness and mass may be different from the initial design values due to various factors. These can include measurement errors (Yamaguchi and Harnpornchai 1993), environmental conditions such as snow accumulation, or equipment replacements in the main structure during maintenance activities (Cao, 2025a). In such cases, tuned vibration absorbers will be "detuned" (Petrini, Giaralis, and Wang 2020). In this section, we conduct a study on the robustness of URPTMD against changes in the properties of the primary structure, where the robustness of URPTMD is compared the robustness of TMD with the same condition.

The robustness of each damper can be evaluated through its ability to resist variations in K_s and/or M_s . In this work, the difference between the actual stiffness and the initial design stiffness of the structure is $\Delta K_s(\%)$, while the difference between the actual mass and the initial design mass of the structure is $\Delta M_s(\%)$. With the assumption that $\Delta K_s(\%)$ and $\Delta M_s(\%)$ change within $[-20\%, +20\%]$ and based on the vibration reduction R_{DMF} , Figs. 8a and 8b present contour maps of the robustness of the URPTMD and TMD against the changes in K_s and M_s with $\mu = 2\%$, respectively. It should be noted that the marked points in these figures are the maximum vibration reduction R_{DMF} of each absorber corresponding to $\Delta K_s = 0$ and $\Delta M_s = 0$ at $\mu = 2\%$.

As shown in Fig. 8, the URPTMD and TMD maintain acceptable effectiveness with a vibration reduction R_{DMF} over 55% when both K_s and M_s rise or drop within $[-20\%, +20\%]$. However, the

Table 4. RMS displacement of the RPTMD and the liquid column with different values of μ .

μ	RMS_{x1}^{RPTMD}	RMS_{x2}^{TLCD}
1.0%	35.77	107.61
1.5%	27.92	74.20
2.0%	22.75	52.62
2.5%	19.59	41.78
3.0%	17.24	33.89
3.5%	16.14	30.11
4.0%	14.24	25.33
4.5%	13.18	22.56
5.0%	12.19	19.87

performance of URPTMD deeply decreases if K_s and M_s rise or drop in opposite directions. In particular, the control performance of URPTMD is reduced to 28.5%, while the effectiveness of TMD drops to only 40%. Based on the formula $\omega_s = \sqrt{K_s/M_s}$, it is important to note that as K_s and M_s vary in opposite directions, the difference in the structure's natural frequency is larger than compared to the case that K_s and M_s vary in the same direction. If K_s increases by 20% and M_s drops by 20%, the variation of the natural frequency of the structure is +22.5%. In contrast, if K_s decreases by 20% and M_s climbs by 20%, the difference in the structural frequency is -18.3%. Hence, a larger change in the structure's natural frequency will result in a deeper decrease in the damper's performance.

It can be concluded that the URPTMD is less robust than the TMD when subjected to changes in K_s and M_s of the structure. This can be explained by the fact that the vibration control ability of the TMD is determined by two tuning parameters (including β_p and ξ_p), whereas the effectiveness of the URPTMD relies on three tuning parameters: two frequency ratios (β_1 and β_2) and ζ . As a result, as K_s and/or M_s vary, the proposed device is detuned across three tuning parameters.

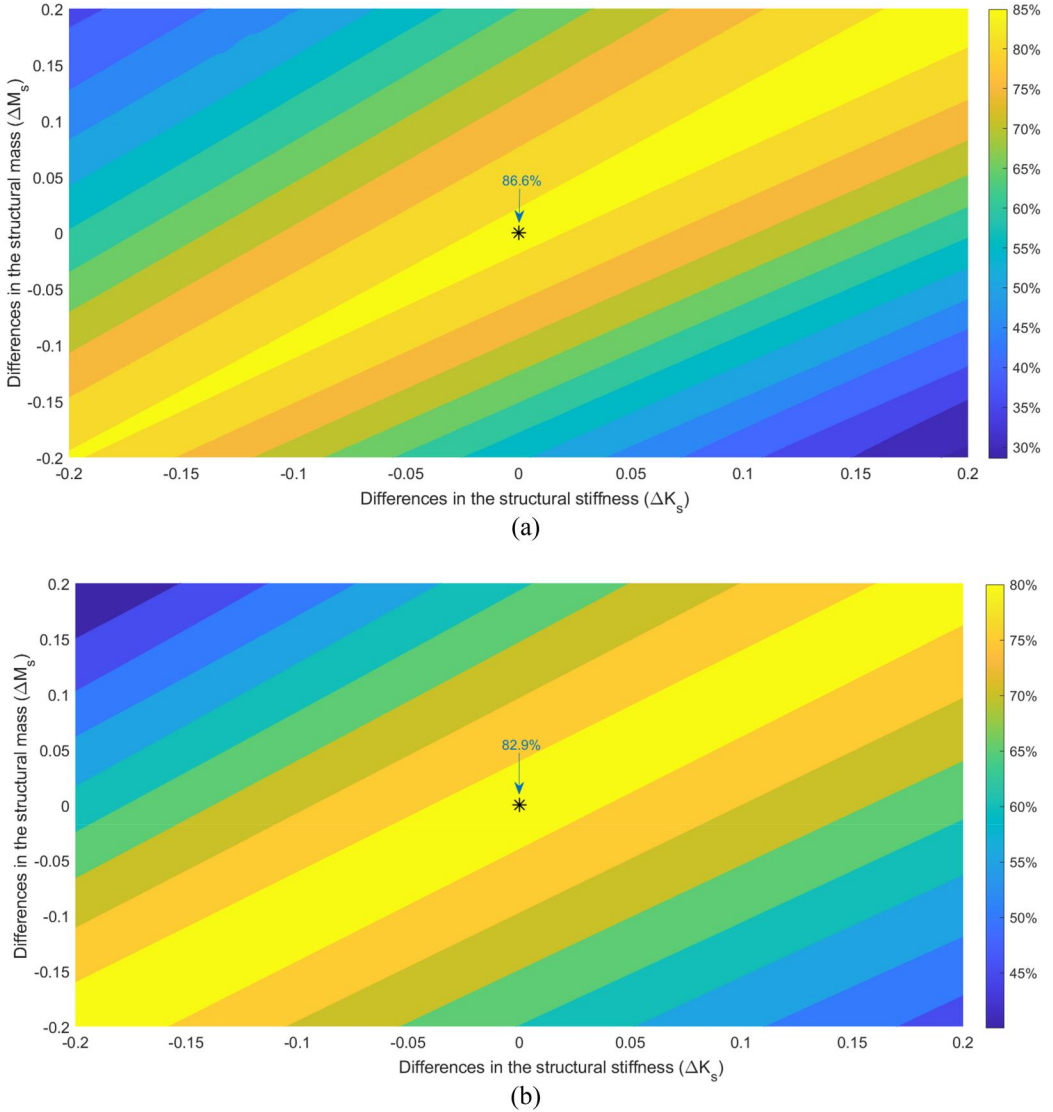


Figure 8. Vibration reduction R_{DMF} of the absorber against changes in K_s and M_s at $\mu = 2\%$: (a) for URPTMD and (b) for TMD.

This detuning can lead to complex interaction among its components in the vibration phases. Consequently, this results in a more significant decrease in control performance of the URPTMD compared to the TMD, which depends on two tuning parameters.

6. Mistuning sensitivity

In practice, due to various factors (e.g. errors in design, manufacturing, or installation), there are always differences (even very small) between the designed optimal values and the actual values of any vibration absorber. This may lead to a decrease in the control effectiveness of the device. Therefore, the mistuning sensitivity related to β_1 , β_2 and ζ of the URPTMD are considered in this section.

6.1. Sensitivity of the head-loss coefficient

Assuming the head-loss coefficient in the URPTMD changes in the range of $[-20\%, +20\%]$ compared with its optimal value. Based on the R_{DMF} index, Fig. 9 describes the sensitivity to changes in the ζ value of the URPTMD. For the sake of comparison, Fig. 9 also presents the sensitivity to variations in ξ_p of the TMD in the same range of $[-20\%, +20\%]$ compared with the optimal ξ_p value. It is found that the sensitivity of the URPTMD to the change in ζ and the sensitivity of the TMD to the variation of ξ_p are small. There is an insignificant difference between the damping sensitivity of the URPTMD and the damping sensitivity of TMD. As reported in Fig. 9, the performance of the URPTMD insignificantly decreases (by only 1.4%) when the head-loss coefficient changes from -20% to 20% compared with its optimal value.

6.2. Mistuning sensitivity

In this subsection, the influence of mistuning on the vibration reduction effectiveness of the optimal URPTMD configuration at $\mu = 2\%$ is explored. It is noted that the URPTMD has two tuning frequency ratios, β_1 and β_2 , in which the tuning ratio β_1 represents for the component having a large mass m_1 and β_2 is for the liquid column with the mass m_2 . Errors in tuning ratios β_1 and β_2 are denoted as $\Delta\beta_1(\%)$ and $\Delta\beta_2(\%)$, respectively. It is assumed that $\Delta\beta_1(\%)$ and $\Delta\beta_2(\%)$ change within $[-20\%, +20\%]$. Figure 10 depicts the contour map of the mistuning sensitivity of the URPTMD when $\Delta\beta_1$ and $\Delta\beta_2$ vary in the range of $[-20\%, 20\%]$. The marked point in Fig. 10 is the maximum vibration control performance of the URPTMD corresponding to $\Delta\beta_1 = 0$ and $\Delta\beta_2 = 0$. It can be seen from Fig. 10 that the mistuning sensitivity of β_1 is higher than that of β_2 . It is found that the mass of m_1 is much larger than the mass of the liquid column (m_2) in the URPTMD. In particular, the optimal URPTMD with $\mu = 2\%$ has $\mu_{21} = \frac{m_2}{m_1} = 0.093$. Therefore, the mass m_1 plays a more vital role compared with the mass m_2 . This is to explain why the mistuning sensitivity of β_1 is greater than that of β_2 .

7. Conclusions

In this work, a URPTMD was proposed to reduce the dynamic response of a SDOF structure under a harmonic force excitation. The effects of the parameters on the fundamental characteristics of a URPTMD showed that URPTMD is significantly effective if the mass ratio μ_{21} chosen is less than 1. Based on the optimal configurations, an optimized URPTMD is more effective than both an optimized TMD and PTMD when they all have the same weight. This means that, for the same level of structural vibration reduction, using a URPTMD instead of a TMD or PTMD can significantly decrease the mass of the absorber added to the structure. Furthermore, the DMF curve of the structure using the URPTMD is relatively flat across a wider frequency range compared with the DMF

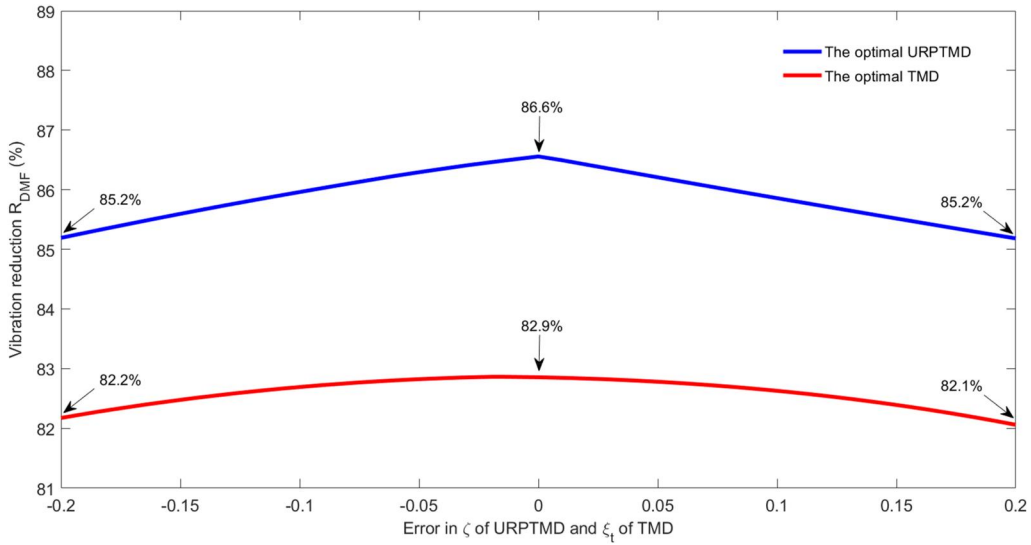


Figure 9. Vibration reduction of URPTMD and TMD when ζ of the URPTMD and ξ_p of the TMD change (with $\mu = 2\%$).

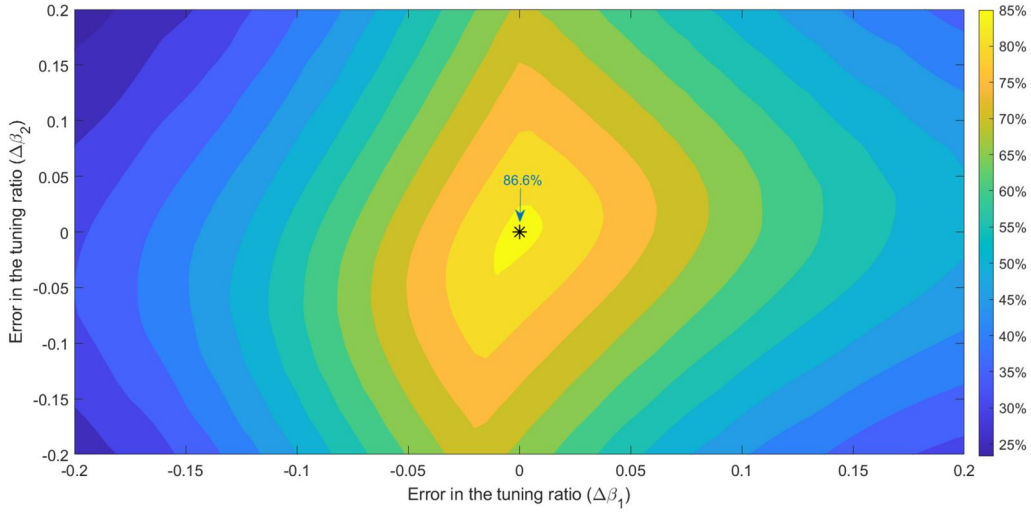


Figure 10. Vibration reduction of URPTMD with $\mu = 2\%$ as β_1 and β_2 vary.

curves of the structure with the TMD or PTMD. Although the optimized URPTMD is less robust than the TMD or PTMD when facing variations in structural stiffness and mass, the damping sensitivity of the optimum URPTMD is similar to that of the optimized TMD.

The unique feature of the URPTMD is that it functions as a passive connectionless vibration absorber. This means it does not need to be connected to the primary structure. By incorporating the TLCD into the RPTMD, the URPTMD is able to generate its own damping coefficient. As a result, it offers easier installation and lower maintenance costs. It is evident that the mass of the liquid column (m_2) in URPTMD is much smaller than the base mass (m_1). However, the presence of the liquid column is crucial for generating the damping coefficient of the URPTMD. This leads to improving the control effectiveness of URPTMD compared to a TMD, PTMD or a traditional RPTMD optimized. Additionally, this innovative type of URPTMD model can be applied to a pendulum tuned mass damper because a rocker pendulum tuned mass damper has the same characteristics as a conventional pendulum tuned mass damper.

In practical applications, the control effectiveness of a URPTMD depends on four design variables: μ_{21} , β_1 , β_2 and ζ . These variables are influenced by the radius of the curved surface, the mass ratio between the TLCD and the RPTMD, the length of the TLCD, and the head-loss coefficient (or the size of the orifice) of the TLCD. Therefore, designing an optimal URPTMD involves properly selecting the radius of the curved surface, the value of μ_{21} , the length of the TLCD, and the size of its orifice. It is clear that the adjustment or tuning of the URPTMD primarily occurs at the TLCD. Furthermore, in a URPTMD, the mass of the TLCD is significantly smaller than that of the RPTMD, and the liquid used in the TLCD is typically water. This provides advantages in terms of manufacturing and installation of the URPTMD.

Although these conclusions are drawn from harmonic force excitation, the proposed damper is also anticipated to be effective under random excitations. Future work will focus on demonstrating the vibration control effectiveness of the URPTMD for complex MDOF structures (e.g. high-rise buildings or towers) subjected to random excitations such as wind and earthquake loadings.

Disclosure statement

No potential conflict of interest was reported by the author(s).

Funding

This research received no specific grant from any funding agency in the public, commercial, or not-for-profit sectors.

ORCID

Huong Quoc Cao  <http://orcid.org/0000-0002-6352-3787>

Data availability statement

All data that support the findings of this study are included within the article.

References

- Araz, O. 2024. "Effect of PGV/PGA Ratio on Seismic-Induced Vibrations of Structures Equipped with Parallel Tuned Mass Dampers considering SSL." *Structures* 68: 107188. <https://doi.org/10.1016/j.istruc.2024.107188>
- Baduidana, M., and A. Kenfack-Jiotsa. 2024. "Parameters Optimization of Three-Element Dynamic Vibration Absorber with Inerter and Grounded Stiffness." *Journal of Vibration and Control* 30 (7-8): 1548–1565. <https://doi.org/10.1177/10775463231164698>
- Bui, H.-L., N.-A. Tran, and H. Q. Cao. 2023. "Active Control Based on Hedge-Algebras Theory of Seismic-Excited Buildings with Upgraded Tuned Liquid Column Damper." *Journal of Engineering Mechanics* 149 (1): 04022091. <https://doi.org/10.1061/JENMDT.EMENG-6821>
- Bui, V.-B., T.-T. Mac, and H.-L. Bui. 2023. "Design Optimization considering the Stability Constraint of the Hedge-Algebras-Based Controller for Building Structures Subjected to Seismic Excitations." *Proceedings of the Institution of Mechanical Engineers, Part I: Journal of Systems and Control Engineering*, 09596518231171960.
- Cao, H. Q. 2023. "Combined Tuned Mass Dampers for Structural Vibration Control." *International Journal of Non-Linear Mechanics* 157: 104550. <https://doi.org/10.1016/j.ijnonlinmec.2023.104550>
- Cao, H. Q. 2025a. "A Comparative Study on the Effectiveness, Robustness and Mistuning Sensitivity of Upgraded Tuned Mass Dampers in Mitigating the Dynamic Response of Civil Structures." *Archive of Applied Mechanics* 95:71. <https://doi.org/10.1007/s00419-025-02781-z>
- Cao, H. Q. 2025b. "Double Tuned Mass Damper with a Grounded Inerter for Structural Vibration Control." *Journal of Vibration and Control* (1-15). <https://doi.org/10.1177/10775463251341758>
- Cao, H. Q., N.-A. Tran, and H.-L. Bui. 1984. "Hedge-Algebras-Based Hybrid Control of Earthquake-Induced Buildings Using Upgraded Tuned Liquid Column Dampers." *Soil Dynamics and Earthquake Engineering* 2024 (182): 108728.
- Cao, Q. H. 2021. "Vibration Control of Structures by an Upgraded Tuned Liquid Column Damper." *Journal of Engineering Mechanics* 147 (9): 04021052. [https://doi.org/10.1061/\(ASCE\)EM.1943-7889.0001965](https://doi.org/10.1061/(ASCE)EM.1943-7889.0001965)

- Den Hartog, J. P. 1985. *Mechanical vibrations*. New York: Dover Publications, Inc.
- Diana, Giorgio, Ferruccio Resta, Diego Sabato, and Gisella Tomasini. 2013. "Development of a Methodology for Damping of Tall Buildings Motion Using TLCN Devices." *Wind and Structures* 17 (6): 629–646. <https://doi.org/10.12989/was.2013.17.6.629>
- Etedali, S., and H. Rakhshani. 2018. "Optimum Design of Tuned Mass Dampers Using Multi-Objective Cuckoo Search for Buildings under Seismic Excitations." *Alexandria Engineering Journal* 57 (4): 3205–3218. <https://doi.org/10.1016/j.aej.2018.01.009>
- Gao, H., K. S. C. Kwok, and B. Samali. 1999. "Characteristics of Multiple Tuned Liquid Column Dampers in Suppressing Structural Vibration." *Engineering Structures* 21 (4): 316–331. [https://doi.org/10.1016/S0141-0296\(97\)00183-1](https://doi.org/10.1016/S0141-0296(97)00183-1)
- Giaralis, A., and F. Petrini. 2017. "Wind-Induced Vibration Mitigation in Tall Buildings Using the Tuned Mass-Damper-Inerter." *Journal of Structural Engineering* 143 (9): 04017127. [https://doi.org/10.1061/\(ASCE\)ST.1943-541X.0001863](https://doi.org/10.1061/(ASCE)ST.1943-541X.0001863)
- Gil-Martín, Luisa María, Juan Francisco Carbonell-Márquez, Enrique Hernández-Montes, Mark Aschheim, and M. Pasadas-Fernández. 2012. "Dynamic Magnification Factors of SDOF Oscillators under Harmonic Loading." *Applied Mathematics Letters* 25 (1): 38–42. <https://doi.org/10.1016/j.aml.2011.07.005>
- Hui, Yi., Zhenhuai Yang, Chao Xia, Yi Su, and Shaopeng Li. 2024. "Study on Vibration Control Performance of Pendulum TMD with Additional Stoppers and Its Application on High-Rise Buildings." *Journal of Wind Engineering and Industrial Aerodynamics* 254: 105926. <https://doi.org/10.1016/j.jweia.2024.105926>
- Kahya, V., and O. Araz. 2019. "A Sequential Approach Based Design of Multiple Tuned Mass Dampers under Harmonic Excitation." *Journal Engineering and Natural Sciences* 37 (1): 225–239.
- Le-Duc, T., Q.-H. Nguyen, and H. Nguyen-Xuan. 2020. "Balancing Composite Motion Optimization." *Information Sciences* 520: 250–270. <https://doi.org/10.1016/j.ins.2020.02.013>
- Li, C., H. Pan, and L. Cao. 2022. "Tuned Tandem Mass Dampers-Inerters for Suppressing Vortex-Induced Vibration of Super-Tall Buildings." *Engineering Structures* 270: 114831. <https://doi.org/10.1016/j.engstruct.2022.114831>
- Marian, L., and A. Giaralis. 2014. "Optimal Design of a Novel Tuned Mass-Damper-Inerter (TMDI) Passive Vibration Control Configuration for Stochastically Support-Excited Structural Systems." *Probabilistic Engineering Mechanics* 38: 156–164. <https://doi.org/10.1016/j.probengmech.2014.03.007>
- McCall, J. 2005. "Genetic Algorithms for Modelling and Optimisation." *Journal of Computational and Applied Mathematics* 184 (1): 205–222. <https://doi.org/10.1016/j.cam.2004.07.034>
- Momtaz, A. A., M. A. Abdollahian, and A. Farshidianfar. 2017. "Study of Wind-Induced Vibrations in Tall Buildings with Tuned Mass Dampers Taking into account Vortices Effects." *International Journal of Advanced Structural Engineering* 9 (4): 385–395. <https://doi.org/10.1007/s40091-017-0174-9>
- Ocak, Ayla, Gebrail Bekdaş, Sinan Melih Nigdeli, Sanghun Kim, and Zong Woo Geem. 2022. "Optimization of Tuned Liquid Damper Including Different Liquids for Lateral Displacement Control of Single and Multi-Story Structures." *Buildings* 12 (3): 377. <https://doi.org/10.3390/buildings12030377>
- Pandey, D. K., and S. K. Mishra. 2021. "Inerter Assisted Robustness of Compliant Liquid Column Damper." *Structural Control and Health Monitoring* 28 (8), p.n/a. <https://doi.org/10.1002/stc.2763>
- Petrini, F., A. Giaralis, and Z. Wang. 2020. "Optimal Tuned Mass-Damper-Inerter (TMDI) Design in Wind-Excited Tall Buildings for Occupants' Comfort Serviceability Performance and Energy Harvesting." *Engineering Structures* 204: 109904. <https://doi.org/10.1016/j.engstruct.2019.109904>
- Prakash, S., and R. S. Jangid. 2022. "Optimum Parameters of Tuned Mass Damper-Inerter for Damped Structure under Seismic Excitation." *International Journal of Dynamics and Control* 10 (5): 1322–1336. <https://doi.org/10.1007/s40435-022-00911-x>
- Rao, S. S. 2017. *Mechanical vibrations*. 6th ed. Pearson Education.
- Samali, B., E. Mayol, K. C. S. Kwok, A. Mack, and P. Hitchcock. 2004. "Vibration Control of the Wind-Excited 76-Story Benchmark Building by Liquid Column Vibration Absorbers." *Journal of Engineering Mechanics* 130 (4): 478–485. [https://doi.org/10.1061/\(ASCE\)0733-9399\(2004\)130:4\(478\)](https://doi.org/10.1061/(ASCE)0733-9399(2004)130:4(478))
- Soltani, P., and A. Deraemaeker. 2022. "Pendulum Tuned Mass Dampers and Tuned Mass Dampers: Analogy and Optimum Parameters for Various Combinations of Response and Excitation Parameters." *Journal of Vibration and Control* 28 (15-16): 2004–2019. <https://doi.org/10.1177/10775463211003414>
- Suthar, S. J., and P. Banerji. 2023. "Inerter-Assisted Pendulum-Tuned Mass Damper for across-Wind Response Control of Tall Buildings." *Engineering Structures* 291: 116489. <https://doi.org/10.1016/j.engstruct.2023.116489>
- Suthar, S. J., and R. S. Jangid. 2022. "Optimal Design of Tuned Liquid Column Damper for Wind-Induced Response Control of Benchmark Tall Building." *Journal of Vibration Engineering & Technologies* 10 (8): 2935–2945. <https://doi.org/10.1007/s42417-022-00528-6>
- Tran, N.-A., and H.-L. Bui. 2025. "Rolling Tuned Mass Damper for Vibration Control of Building Structures Subjected to Earthquakes: A Comparative Study." *Soil Dynamics and Earthquake Engineering* 194: 109376. <https://doi.org/10.1016/j.soildyn.2025.109376>

- Tran, N.-A., H.-L. Bui, and Q.-H. Cao. 2024. “U-Shaped and V-Shaped Tuned Liquid Column Dampers in Vibration Reduction of Earthquake-Induced Buildings: A Comparative Study.” *Structures* 65: 106669. <https://doi.org/10.1016/j.jistruc.2024.106669>
- Tran, N.-A., V.-B. Bui, and Q.-H. Cao. 2025. “High Control Performance of Tuned Two-Mass Damper Using Grounded Inerters for Vibration Control of Civil Structures.” *Mechanics Based Design of Structures and Machines*, 1–24. <https://doi.org/10.1080/15397734.2025.2509255>
- Tran, Ngoc-An, Van-Bao Hoang, Hai-Le Bui, and Huong Quoc Cao. 2025. “Upgraded Double Tuned Mass Dampers for Vibration Control of Structures under Earthquakes.” *Computers & Structures* 310: 107700. <https://doi.org/10.1016/j.compstruc.2025.107700>
- Varadarajan, N., and S. Nagarajaiah. 2004. “Wind Response Control of Building with Variable Stiffness Tuned Mass Damper Using Empirical Mode Decomposition/Hilbert Transform.” *Journal of Engineering Mechanics* 130 (4): 451–458. [https://doi.org/10.1061/\(ASCE\)0733-9399\(2004\)130:4\(451\)](https://doi.org/10.1061/(ASCE)0733-9399(2004)130:4(451))
- Vellar, L. S, P. K. Gupta, and R. S. Jangid. 2019. “Robust Optimum Design of Multiple Tuned Mass Dampers for Vibration Control in Buildings Subjected to Seismic Excitation.” *Shock and Vibration* 2019: 1–9.
- Wang, L., W. Shi, and Y. Zhou. 2022. “Adaptive-Passive Tuned Mass Damper for Structural Aseismic Protection Including Soil–Structure Interaction.” *Soil Dynamics and Earthquake Engineering* 158: 107298. <https://doi.org/10.1016/j.soildyn.2022.107298>
- Wang, Qinhua, Nayan Deep Tiwari, Haoshuai Qiao, and Quan Wang. 2020. “Inerter-Based Tuned Liquid Column Damper for Seismic Vibration Control of a Single-Degree-of-Freedom Structure.” *International Journal of Mechanical Sciences* 184: 105840. <https://doi.org/10.1016/j.ijmecsci.2020.105840>
- Wang, Wenxi, Tianfu Yu, Zhilin Yang, Sheng Chen, Xugang Hua, and Ou Yang. 2023. “Optimum Design of Pendulum Tuned Mass Dampers Considering Control Performance Degradation from Damper Connection.” *Journal of Structural Engineering* 149 (12): 04023163. <https://doi.org/10.1061/JSENDH.STENG-12312>
- Wu, Jong-Cheng, Ming-Hsiang Shih, Yuh-Yi Lin, and Ying-Chang Shen. 2005. “Design Guidelines for Tuned Liquid Column Damper for Structures Responding to Wind.” *Engineering Structures* 27 (13): 1893–1905. <https://doi.org/10.1016/j.engstruct.2005.05.009>
- Yalla, S. K., and A. Kareem. 2000. “Optimum Absorber Parameters for Tuned Liquid Column Dampers.” *Journal of Structural Engineering* 126 (8): 906–915. [https://doi.org/10.1061/\(ASCE\)0733-9445\(2000\)126:8\(906\)](https://doi.org/10.1061/(ASCE)0733-9445(2000)126:8(906))
- Yamaguchi, H., and N. Harnpornchai. 1993. “Fundamental Characteristics of Multiple Tuned Mass Dampers for Suppressing Harmonically Forced Oscillations.” *Earthquake Engineering & Structural Dynamics* 22 (1): 51–62. <https://doi.org/10.1002/eqe.4290220105>
- Yang, Jann N., Anil K. Agrawal, Bijan Samali, and Jong-Cheng Wu. 2004. “Benchmark Problem for Response Control of Wind-Excited Tall Buildings.” *Journal of Engineering Mechanics* 130 (4): 437–446. [https://doi.org/10.1061/\(ASCE\)0733-9399\(2004\)130:4\(437\)](https://doi.org/10.1061/(ASCE)0733-9399(2004)130:4(437))
- Zuo, L. 2009. “Effective and Robust Vibration Control Using Series Multiple Tuned-Mass Dampers.” *Journal of Vibration and Acoustics* 131 (3): 11–11. <https://doi.org/10.1115/1.3085879>

Appendix A.

Newmark’s average acceleration method

The Newmark average acceleration method is a numerical integration technique utilized to solve specific differential equations. It is commonly employed for the numerical evaluation of the dynamic response of structures. This method is an implicit time integration technique that calculates displacements, velocities, and accelerations at discrete time steps, assuming a linear variation of acceleration within each step. We begin the derivation of Newmark’s method by considering the second-order differential equations of motion of the URPTMD-structure system. They are Eqs. (8a-8c) and can be written in a matrix form as follows:

$$\mathbf{M}\ddot{\mathbf{X}} + \mathbf{C}\dot{\mathbf{X}} + \mathbf{K}\mathbf{X} = \mathbf{F}, \quad (\text{A1})$$

where the displacement vector \mathbf{X} is defined as $\mathbf{X} = \begin{bmatrix} X_s \\ x_1 \\ x_2 \end{bmatrix}$, and $\dot{\mathbf{X}}$ and $\ddot{\mathbf{X}}$ are velocity and acceleration vectors, respectively. The external force vector \mathbf{F} is determined as $\mathbf{F} = \begin{bmatrix} F_0 \\ 0 \\ 0 \end{bmatrix} e^{j\omega t}$, and it is

a function of time. The mass \mathbf{M} , damping \mathbf{C} and stiffness \mathbf{K} matrices of the system are

$$\mathbf{M} = \begin{bmatrix} M_s & 0 & 0 \\ m_1 + m_2 & m_1 + m_2 & \gamma m_2 \\ \gamma m_2 & \gamma m_2 & m_2 \end{bmatrix}, \mathbf{C} = \begin{bmatrix} C_s & 0 & 0 \\ 0 & 0 & 0 \\ 0 & 0 & \frac{m_2 \zeta}{2L} |\dot{x}_2(t)| \end{bmatrix}, \mathbf{K} = \begin{bmatrix} K_s & -k_{eq} & 0 \\ 0 & k_{eq} & 0 \\ 0 & 0 & m_2 \frac{2g}{L} \end{bmatrix} \quad (\text{A2})$$

The Newmark method approximates the displacements and velocities at time $t_{n+1} = t_n + \Delta t$ based on the known values at time t_n , in which Δt is time step size. At the initial time ($t_0 = 0$), we have the displacements are equal to zero ($\mathbf{X}_0 = 0$) and the velocities are equal to zero ($\dot{\mathbf{X}}_0 = 0$). It is important to note that the matrix \mathbf{C} depends on $|\dot{x}_2(t)|$. Thus, the damping matrix \mathbf{C} is also changed over time. When we know $\dot{\mathbf{X}}_0$, this means that \mathbf{C}_0 (the damping matrix at time t_0) is also determined. The acceleration components ($\ddot{\mathbf{X}}_0$) of the system are obtained by solving the following equation for $\ddot{\mathbf{X}}_0$

$$\mathbf{M}\ddot{\mathbf{X}}_0 + \mathbf{C}_0\dot{\mathbf{X}}_0 + \mathbf{K}\mathbf{X}_0 = \mathbf{F}_0 \quad (\text{A3})$$

Assume that \mathbf{X}_n , $\dot{\mathbf{X}}_n$, $\ddot{\mathbf{X}}_n$ and \mathbf{C}_n are known at t_n . The displacements and velocities at time $t_{n+1} = t_n + \Delta t$ are determined as follows.

For the displacements:

$$x_{n+1}^i = x_n^i + \Delta t \dot{x}_n^i + \frac{\Delta t^2}{2} \left[(1 - 2\beta) \ddot{x}_n^i + 2\beta \ddot{x}_{n+1}^i \right]. \quad (\text{A4})$$

For the velocities:

$$\dot{x}_{n+1}^i = \dot{x}_n^i + \Delta t \left[(1 - \gamma) \ddot{x}_n^i + \gamma \ddot{x}_{n+1}^i \right]. \quad (\text{A5})$$

In the above equations, x_{n+1}^i represents the i^{th} component of the displacement vector \mathbf{X} and the subscript “ $n + 1$ ” is at time t_{n+1} . The sign ‘ \cdot ’ represents differentiation with respect to time t . For the Newmark average acceleration method, the parameters include $\beta = \frac{1}{4}$ and $\gamma = \frac{1}{2}$. Thus, for the displacements, Eq (A4) becomes:

$$x_{n+1}^i = x_n^i + \Delta t \dot{x}_n^i + \frac{\Delta t^2}{4} \left(\ddot{x}_n^i + \ddot{x}_{n+1}^i \right), \quad (\text{A6})$$

and for the velocities, Eq (A5) becomes:

$$\dot{x}_{n+1}^i = \dot{x}_n^i + \frac{\Delta t}{2} \left(\ddot{x}_n^i + \ddot{x}_{n+1}^i \right). \quad (\text{A7})$$

To solve the equation of motion of the system, we need to express x_{n+1}^i and \dot{x}_{n+1}^i in terms of \ddot{x}_{n+1}^i . For the displacements from Eq. (A6), we have

$$x_{n+1}^i = \bar{x}_n^i + \frac{\Delta t^2}{4} \ddot{x}_{n+1}^i, \quad (\text{A8})$$

with

$$\bar{x}_n^i = x_n^i + \Delta t \dot{x}_n^i + \frac{\Delta t^2}{4} \ddot{x}_n^i. \quad (\text{A9})$$

For the velocities from Eq (A7), we have

$$\dot{x}_{n+1}^i = \dot{x}_n^i + \frac{\Delta t}{2} \ddot{x}_{n+1}^i, \quad (\text{A10})$$

with

$$\dot{\tilde{x}}_n^i = \dot{x}_n^i + \frac{\Delta t}{2} \ddot{x}_n^i. \quad (\text{A11})$$

Here, \bar{x}_n^i and $\dot{\tilde{x}}_n^i$ contain all known terms at time t_n . For the URPTMD-structure system, the equation of motion at time t_{n+1} is given by

$$\mathbf{M}\ddot{\mathbf{X}}_{n+1} + \mathbf{C}_n\dot{\mathbf{X}}_{n+1} + \mathbf{K}\mathbf{X}_{n+1} = \mathbf{F}_{n+1}. \quad (\text{A12})$$

By substituting Eqs. (A8) and (A10) into Eq. (A12), we have

$$\mathbf{M}\ddot{\mathbf{X}}_{n+1} + \mathbf{C}_n\left(\dot{\tilde{\mathbf{X}}}_n + \frac{\Delta t}{2}\ddot{\mathbf{X}}_{n+1}\right) + \mathbf{K}\left(\bar{\mathbf{X}}_n + \frac{\Delta t^2}{4}\ddot{\mathbf{X}}_{n+1}\right) = \mathbf{F}_{n+1}. \quad (\text{A13})$$

The above equation can be simplified by

$$\left(\mathbf{M} + \frac{\Delta t}{2}\mathbf{C}_n + \frac{\Delta t^2}{4}\mathbf{K}\right)\ddot{\mathbf{X}}_{n+1} = \mathbf{F}_{n+1} - \mathbf{C}_n\dot{\tilde{\mathbf{X}}}_n - \mathbf{K}\bar{\mathbf{X}}_n. \quad (\text{A14})$$

Now, we solve Eq. (A.14) for the accelerations at time t_{n+1}

$$\ddot{\mathbf{X}}_{n+1} = \left(\mathbf{M} + \frac{\Delta t}{2}\mathbf{C}_n + \frac{\Delta t^2}{4}\mathbf{K}\right)^{-1} \left(\mathbf{F}_{n+1} - \mathbf{C}_n\dot{\tilde{\mathbf{X}}}_n - \mathbf{K}\bar{\mathbf{X}}_n\right). \quad (\text{A15})$$

After having $\ddot{\mathbf{X}}_{n+1}$, one can compute the displacements (\mathbf{X}_{n+1}), velocities ($\dot{\mathbf{X}}_{n+1}$) and the damping matrix (\mathbf{C}_{n+1}) at time t_{n+1} by using Eqs. (A8, A10 and A2 for the matrix \mathbf{C}). It should be noted that the average acceleration method is unconditionally stable. This means that it remains stable for any time step size Δt .

Appendix B.

The TMD-structure system

An analytical model of the main structure equipped with a TMD subjected to an external excitation is shown in Fig. B1. TMD has the mass m_{tmd} , the stiffness k_{tmd} and the damping coefficient c_{tmd} . The equations of motion of the TMD-structure are given as follows:

$$m_{tmd}\ddot{x}_{tmd}(t) + c_{tmd}\dot{x}_{tmd}(t) + k_{tmd}x_{tmd}(t) = -m_{tmd}\ddot{X}_s(t), \quad (\text{B1})$$

$$M_s\ddot{X}_s(t) + C_s\dot{X}_s(t) + K_sX_s(t) - c_{tmd}\dot{x}_{tmd}(t) - k_{tmd}x_{tmd}(t) = F(t) \quad (\text{B2})$$

where x_{tmd} is the displacement of the mass m_{tmd} relative to M_s .

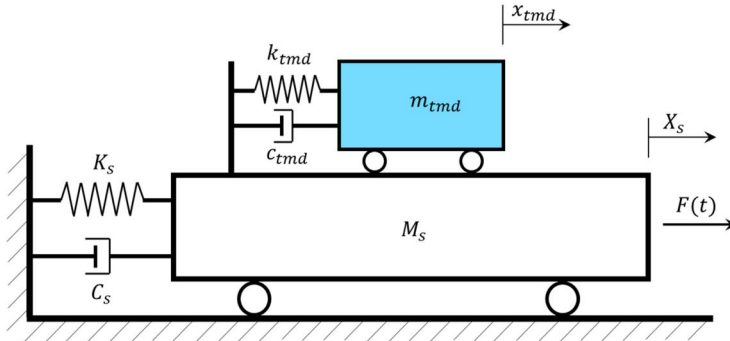


Figure B1. Analytical model of the TMD-structure system.

The natural frequency of the TMD is

$$\omega_{tmd} = \sqrt{\frac{k_{tmd}}{m_{tmd}}}. \quad (\text{B3})$$

The damping ratio of the TMD is

$$\xi_{tmd} = \frac{c_t}{2m_{tmd}\omega_{tmd}}. \quad (\text{B4})$$

The mass ratio between the TMD and the structure is

$$\mu_{tmd} = \frac{m_{tmd}}{M_s}. \quad (\text{B5})$$